Self-collimation in photonic crystals with anisotropic constituents

J. W. Haus[1], M. Siraj[1], P. Prasad[2], and P. Markowicz[2*]

[1] *Electro-Optics Program, University of Dayton, Dayton, OH 45469-0245*

[2] *State University of New York at Buffalo, Institute for Lasers, Photonics and Biophotonics, Buffalo, NY 14260-3000*

Received August 15, 2007

In a photonic crystal composed of anisotropic constituents we quantify the range of input angles and the degree of collimation of the beam inside the crystal. The optical properties of a photobleached 4-dimethylamino-N-methyl-4-stilbazolium-tosylate (DAST) crystal are used in our model to demonstrate the efficacy of the self-collimation features.

OCIS codes: 160.1190, 160.4330.

Photonic crystals (PhCs) possess unique dispersion properties that can be exploited to enable novel photonic applications. These properties can also be used to significantly improve the performance of existing photonic devices. Many applications of PhCs such as waveguides, PC fibers and photonic cavities have been explored by using the presence of a photonic bandgap over a desired frequency range with a defect incorporated in the structure to allow only a desired mode with its symmetry to propagate. This strategy often requires a large index contrast between materials to create the band gap in the first place and limit the materials that can be used for the devices. On the other hand, many phenomena such as negative refraction, superprism, super-resolution, and slow light have been demonstrated based on unique spatial and temporal dispersion properties of a PhC[1] and they are often observable with materials having a low index contrast.

In this paper we investigate self-collimation, another dispersion-related phenomenon of PhCs, that is manifested to some degree in all PhCs. In free space or homogeneous materials propagating electromagnetic waves spread due to diffraction effects, but a PhC in the region of self-collimation has essentially no diffraction and input beams spread over a range of input angles are collimated into a single direction. The phenomenon of beam-like propagation without divergence is important to many applications, including optical interconnects in an integrated circuit. Self-collimation provides a solution to beam control that does not require additional fabrication steps and can be used in conjunction with additional effects to further tailor the application needs.

The shape of the PhC isofrequency dispersion surface is the essential feature determining the self-collimation and can be optimized and manipulated, for instance, by lattice symmetry, material parameters and the geometry shape of the constituents[2]. In constituent isotropic materials, the electric polarization and refractive index are independent of the wave propagation direction; however, in anisotropic materials, both polarization and refractive index depend on the wave propagation direction. Therefore the dispersion surfaces of PhCs made with anisotropic constituent materials provide another degree of freedom for improving the performance.

Anisotropic materials in the PhC were first studied by Zabel and Stroud[3] in 1993. The authors demonstrated that the anisotropy can reduce the band gap of PhC by breaking the degeneracies of bands with different polarizations. They even found a case where sufficient anisotropy would close the gap altogether. In 1998, Li *et al.* reported a large absolute band gap in two dimensional (2D) PhCs made of anisotropic materials[4,5]. Recently, Alagappan et al. extensively explored anisotropic materials and among other results, reported the decoupling of the two polarizations on 2D PhC made of anisotropic materials[6].

In this paper we study PhCs with mixtures of anisotropic materials; both the inclusions and the background may be anisotropic. To demonstrate the significance of anisotropic materials we report the results on self-collimating phenomena. In particular we examine the degree of self-collimation versus the range of input angles. Moreover, we identified a potential candidate for realizing such an anizotropic medium, an organic ionic salt crystal with the acronym 4-dimethylamino-N-methyl-4-stilbazolium-tosylate (DAST). Photo-induced chemical reactions can be used to change the optical properties[7] and the refractive index of this material. However, the index contrast is modest and thus does not produce a full band gap. In DAST either or both constituent materials can be anisotropic and the anisotropy can be controlled to some degree by the radiation dose. Our choice of DAST is motivated by planned experiments on Terahertz (THz) generation, where the nonlinear optical rectification is very strong with d_{111} approximately 500 pm/V near a wavelength of 1500 nm[8,9].

In the present study we model a 2D square lattice photonic crystal with anisotropic dielectric constants. The specific dielectric parameters used in this paper are motivated by recent results on DAST, which is a biaxial anisotropic crystal. DAST undergoes a large change of its refractive indices when irradiated with visible light. By using the multiple-beam interference laser lithography a periodic structure can be written into the host material. By the choice of beam geometries the volume that is bleached can be either an inclusion-like region or a host medium region. To illustrate the dispersion effects of the refractive index ellipsoid we simplify the topology

1671-7694/2007/090527-04

of the structure by using circular rods for the shape of the material embedded in the host. Bleached DAST rod-like cylinders are periodically embedded in the non-bleached DAST host material. Bleached and non-bleached regions are both anisotropic, although the bleached material is nearly isotropic.

The data in Table 1 illustrate the large changes induced in the refractive index for bleached and unbleached DAST. DAST crystals can be grown in relatively large sizes with good optical quality[7] and the combinations of low dielectric constant and high nonlinearity make DAST crystals interesting materials for high speed modulation and frequency mixing applications, including generation and detection of THz radiation[10]. We can exploit the large change of the refractive index to modify the isofrequency dispersion curves and in particular, the angular range for acceptable self-collimation in the PhC can be improved.

Maxwell's equations can be reduced to scalar equations under the condition that a principal axis is parallel to the rod axis. In this case we assume the spatially periodic, dielectric function has the form

$$\tilde{\tilde{\varepsilon}}(\vec{x}) = \begin{bmatrix} \varepsilon_{xx} & \varepsilon_{xy} & 0 \\ \varepsilon_{yx} & \varepsilon_{yy} & 0 \\ 0 & 0 & \varepsilon_{zz} \end{bmatrix}. \quad (1)$$

The axis of the rods is along the z-axis and the other two axes can be rotated with respect to the x- and y-axes. For 2D in-plane propagation of waves with the dielectric tensor in Eq. (1), Maxwell's equations are reduced to scalar wave equations. For the E-field parallel to the rods (along the axis labeled z), the wave equation takes the scalar form

$$\nabla_{\perp}^2 E + k^2 \varepsilon_{zz} E = 0. \quad (2)$$

This has the same solutions as the isotropic case and will be used as a comparison case in this paper. For the H-field parallel to the rods the scalar wave equation takes the form

$$\vec{\nabla}_{\perp} \cdot \tilde{\tilde{\eta}} \vec{\nabla}_{\perp} H + k^2 H = 0. \quad (3)$$

The operators are restricted to the x-y plane and k is the free space wave number. The inverse of the rank 2 sub-matrix is given by

$$\tilde{\tilde{\eta}} = \begin{bmatrix} \varepsilon_{xx} & \varepsilon_{xy} \\ \varepsilon_{yx} & \varepsilon_{yy} \end{bmatrix}^{-1}. \quad (4)$$

Equation (3) has contributions mixing the diffraction in the x-y plane which can dramatically alter the spatial dispersion. We concentrate here on the solution of Eq. (3) by using the plane-wave expansion method. The wave equation in the plane-wave form is written as

$$\sum_{\vec{G}'} (\vec{G} - k) \cdot \tilde{\tilde{\eta}} (\vec{G} - \vec{G}') \cdot (\vec{G}' - k) H_{\vec{G}'} + k^2 H_{\vec{G}} = 0. \quad (5)$$

The radius of the circular cylinders is r and the lattice constant is a. As usual, the lattice constant is used to scale the cylinder radius,

$$\eta_{ij}(\vec{G}) = \left(\frac{\pi r^2}{a^2} \Delta\eta_{ij} + \eta_{ij}(\text{host}) \right) \delta_{\vec{G},\vec{0}} + 2\Delta\eta_{ij} \frac{\pi r^2}{a^2} \frac{J_1(Gr)}{Gr}, \quad (6)$$

where $\Delta\eta_{ij} = \eta_{ij}(\text{rod}) - \eta_{ij}(\text{host})$ and $i, j = x, y$.

The solution of Eq. (5) and the corresponding isotropic medium case are straightforward. We construct isofrequency curves for specific case and discuss the implication for self-collimation in the following section. In particular we examine the second band, which has a self-collimation feature.

Our discussion is restricted to a 2D square lattice of circular rods with radii varied from $r = 0.1a$ to $0.5a$, where a is the period of the lattice. The DAST crystal index parameters are varied for n_1 between 2.55 and 1.64 and for n_2 between 1.78 and 1.62, respectively, for the background medium going from the unbleached to the bleached states. We choose the condition $\varepsilon_{zz} = n_z^2$ with $n_z = 2.55$ for an isotropic response (i.e., the E-field is parallel to the rods, which are oriented along the principal axis for n_1). The refractive indices of the bleached holes at the wavelength of 633 nm are $n_1 = 1.64$ and $n_2 = 1.62$, which correspond to a nearly isotropic medium. The hole radius and the background anisotropy are varied to optimize the angular dispersion for the largest incident angle that can be self-collimated inside the crystal. In the following we shall present dispersion surfaces of this crystal. The birefringence ratio defined as n_1/n_2 is 1.43 for unbleached DAST at 663 nm. For bleached DAST the birefringence ratio is reduced to 1.01.

In Fig. 1 we present the isofrequency surfaces for the

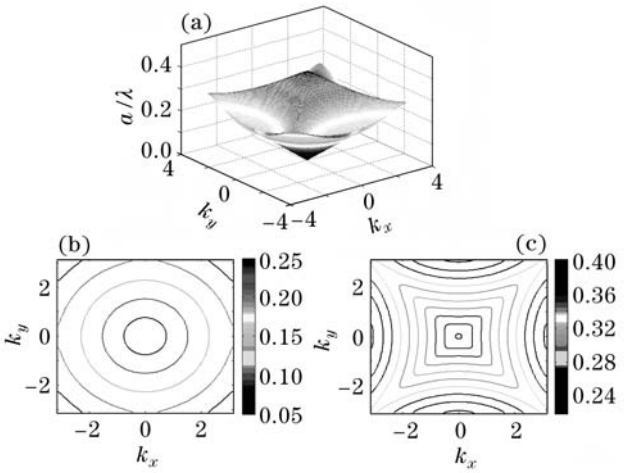

Fig. 1. Isofrequency representation for bands 1 and 2 for a square lattice with isotropic materials. (a) 3D view of the first two bands; (b) and (c) contours of bands 1 and 2. The refractive indices are $n_{\text{rod}} = 1.62$ and $n_{\text{host}} = 2.55$, and the radius of the rods is $r = 0.2a$.

Table 1. Principal Refractive Indices for DAST[7]

λ	$n_1(\|\|a)$		$n_2(\|\|b)$		$n_3(\|\|c)$	
(nm)	Crystal	Bleached	Crystal	Bleached	Crystal	Bleached
633	2.550	1.641	1.784	1.616	1.597	1.629
830	2.351	1.613	1.659	1.603	1.583	1.611
1300	2.166	1.591	1.620	1.614	1.575	1.592
1500	2.138	1.580	1.614	1.608	1.571	1.588

first and second band of a PhC with the rods oriented parallel to the principal axis of the refractive index ellipsoid labeled 1 and the E-field parallel to the rods. The cylinder radius is $0.2a$, where a is the lattice constant. This is equivalent to an isotropic square lattice and is shown in Fig. 1(a). The wave vector is scaled so that the first Brillouin zone lines in the range $(-\pi, \pi)$ for each component. By comparison the same dispersion surfaces in Fig. 1(b) and (c) are shown as contours. The first band has an isotropic propagation at low frequencies with circular isofrequency curve features; while the second band has a square, pyramidal shape with slight curvature and rounded edges. There is a frequency where the curvature is minimized over a wide range of input angles and this constitutes the optimal isofrequency value for self-collimation in the photonic crystal. The extent of self-collimation is quantified by examining the group velocity (also the direction of power flow), which is determined by the gradient of the frequency in k-space,

$$\vec{v}_{\rm g} = \vec{\nabla}_{\vec{k}}\omega. \tag{7}$$

The magnitude of the group velocity index near the band center for the first band is 2.0 over most of the Brillouin zone, except near the band edges, and the group velocity magnitude for the second band is also 2.0 over most of the Brillouin zone region. By inspecting the isofrequency surfaces, the pyramidal-shaped second band has a region where the crystal self-collimates an incident beam over a range of angles.

When such a PhC is illuminated within frequency range of first band, the isofrequency contours are circularly shaped and incident light on the PhC undergoes usual refraction when the wave vector is sufficiently far from the Brillouin zone boundary. However, second band isofrequency surfaces have a flattened, squarer shape for a range of frequencies. For the isofrequency contour $a/\lambda = 0.38$, the beam is collimated for the range of the scaled transverse wave vectors, k_y, lying between about -0.4 and $+0.4$. The normal value of the wave vector in the PhC changes by about 0.5% and the group velocity varies from vertical by about $\theta_{\rm g} < 1^\circ$ (i.e., $\sin\theta_{\rm g} = v_{{\rm g}y}/|v_{\rm g}|$). The range of the scaled transverse wave vector k_y lies between about -0.4 and $+0.4$, for light in the PhC propagating within an angle of 1° of the x-axis. The incident angle is determined by using Snell's law in the form $\frac{a}{\lambda}\sin(\theta_{\rm in}) = \frac{k_y}{2\pi}$, the calculated maximum input angle for $a/\lambda = 0.38$ and $k_y = 0.4$ is about 9.6°. In other words, an incident light beam with a divergence up to 9.6° can be self-collimated in the PhC to within 1°. It is desirable to have a larger flatter surface so the acceptable incident angle will be larger and therefore incident light with a higher divergence can be collimated in the PhC.

We now turn our attention to study the effect of anisotropic dielectrics on the self-collimation of light in the PhC. We first determine the maximum input angle that is collimated to within a certain angle for a cylinder radius $0.2a$, as a function of the anisotropy ratio. The birefringence ratio, n_1/n_2, is changed only for the background refractive indices while keeping the cylinder birefringence ratio constant. Figures 2(a)—(c) show the second-band contours while varying the index ratio. The curvature of the isofrequency curvature along the k_x axis

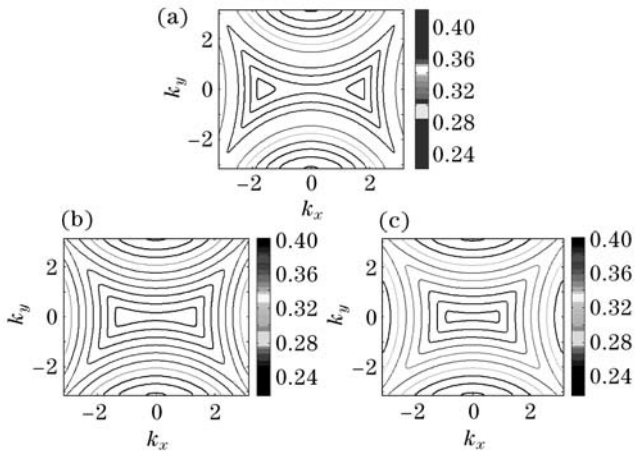

Fig. 2. Second band isofrequency contours. The index n_1 is fixed at 2.55 and the values of n_2 are (a) 1.7, (b) 1.9, (c) 2.2. $r = 0.2a$.

is much larger than the curvature along the k_y axis in our figures. To achieve high collimation of the optical beams in the PhC over the largest range of incident divergence angles the propagation closer to the x-axis is desirable. We determine the angles of refraction using Snell's law. For an incident beam propagating close to the x-axis, a range of transverse wave vectors, k_y, is used to determine the degree of self-collimation. The self-collimation of the beam is defined in terms of the group velocity, as discussed in the previous paragraph. The values of the refractive index in Figs. 2(a)—(c) are $n_2 = 1.7$, 1.9, and 2.2. As n_2 decreases, the shape of the isofrequency curves are elongated more along the x-axis. The contours parallel to the k_y axis for $a/\lambda = 0.38$ have sufficiently flat contours over a range of frequencies and the range becomes smaller as the birefringence ratio is reduced toward the isotropic case. The curvature of the isofrequency contours is much greater for propagation along the x-axis until the birefringence is sufficiently reduced where it approaches the value quoted above for an isotropic material, as in Fig. 1(c).

In Fig. 3 the dependence of the angular deviation of the group velocity from normal is plotted against the corresponding input angle. These data are extracted from the isofrequency curve by computing the gradient of the frequency. The line is nearly linear from normal incidence (0) to close to the maximum deviation of $\theta_{\rm g}$. At an input angle near 25° the deviation angle is about 6°, while

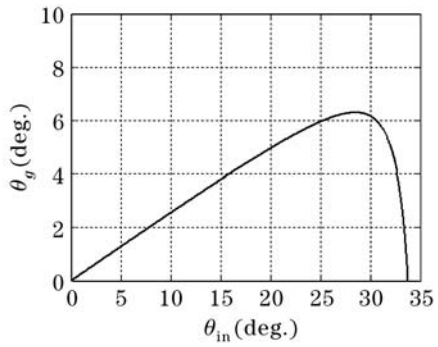

Fig. 3. Isofrequency curve for the case $r = 0.15a$ showing the maximum of the angular deviation of the group velocity.

at 12.5° the deviation is about 3°. Exploiting a region where large input angle ranges are found that can lead to a larger deviation angle, as in Fig. 3.

We explore the relationship between the input angles and the angular deviation of the group velocity for a range of birefringence ratios in Fig. 4. As in Fig. 3 for a fixed frequency we extract the maximum incidence angle from air to the PhC where the group velocity deviates from the x direction. The results for a range of parameters are summarized in Fig. 4 for the fixed frequency $a/\lambda = 0.38$ and the fixed hole radius $0.2a$. The curves are generated by adjusting the frequency and determining the maximum of $\theta_{\rm g}$. The maxima of $\theta_{\rm g}$ are almost linearly related to the input angles at the maximum. The larger anisotropies do better for larger input angles by better collimating a divergent input beam. The solid line is the isotropic case for a rod index of 2.55.

The cylinder radius is another strong parameter affecting the dispersion surfaces. In Fig. 5 we summarize the effect of the cylinder radii by plotting the maximum angular deviation of the group velocity from the surface normal. Two cases of self-collimation are plotted here. The solid curve is for the isotropic medium case and the dashed curves are for the anisotropic medium case. There are two curves for each case, the upper curve shows isofrequency curves with a maximum deviation of 6.5° and the lower curve is deduced from data with a maximum deviation of 4.5°. An input angle of 30° was found for the anisotropic case and a cylinder radius around $r = 0.2a$. The anistropic and the isotropic cases are nearly identical for a radius of $0.5a$. The maximum deviation for isotropic media can be maintained for a range of radii between $0.2a$ and $0.4a$. Larger input angles are found for cylinder radii between $0.1a$ and $0.3a$.

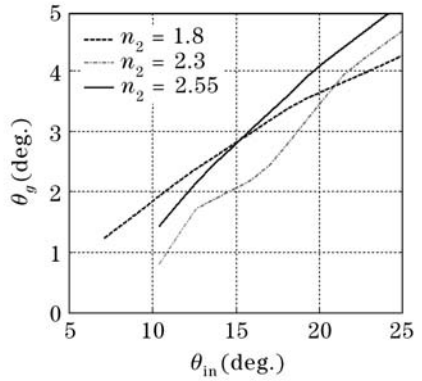

Fig. 4. Maximum angular deviation of the group velocity versus the incident angle at that point for selected values of n_2. Cylinder radii are $r = 0.2a$.

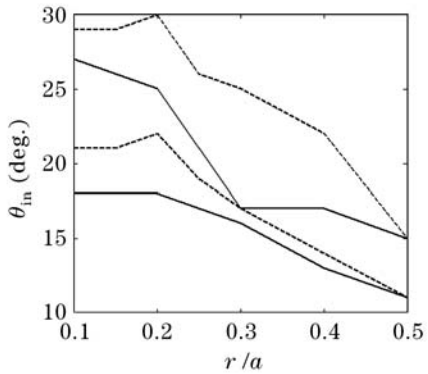

Fig. 5. Input angle for the maximum deviation of the group velocity from normal versus the scaled cylinder radius. The dashed lines correspond to data for the anisotropic PhC and the solid curve is data for the isotropic PhC. The upper curves are for the maximum deviation of 6.5°, and the lower for 4.5°.

In conclusion, for relatively modest refractive index changes, the dispersion surfaces of anisotropic photonic crystals may be greatly distorted from those of a homogeneous medium. The parameters we used in our calculations are within ranges that have already been achieved for DAST in the laboratory. This paper demonstrated how the use of anisotropy for the constituents can be applied to increase the range of input angles that are self-collimated. We used cylindrical rods on a square lattice embedded in a host medium, both of which could be anisotropic. The self-collimation is effective for two PhC geometries. In both cases the E-field parallel to the n_1 principal axis, while for the isotropic case the rods are aligned with the n_1 principal axis and for the anisotropic case the rods parallel to the n_2 principal axis. The precise geometric structure of the photonic crystal constituents modifies the results here, but the general results are maintained. Also the rotation of the principle axes of the anisotropic media relative to the symmetry axes of the photonic crystals can be applied to further engineer the dispersion surfaces for a variety of applications. The strong second-order nonlinearity of the DAST crystal can be further used to generate a strong THz signal by mixing two waves inside the sample. By managing the dispersion inside the crystal two beams incident at different angles can be collimated inside the PhC to assure a small walkoff of the beams.

J. W. Haus' e-mail address is jwhaus@udayton.edu.
∗Current address: Corporate Research Process Laboratory, 3M Center, St. Paul, MN 55144-1000.

References

1. S. Noda and T. Baba, (eds.) *Roadmap to Photonic Crystals* (Kluver, Boston, 2003).
2. H. Kosaka, T. Kawashima, A. Tomita, M. Notomi, T. Sato, and S. Kawakami, Appl. Phys. Lett **74,** 1212 (1999).
3. I. H. H. Zabel and D. Stroud, Phys. Rev. B **48,** 5004 (1993).
4. Z.-Y. Li, B.-Y. Gu, and G.-Z. Yang, Phys. Rev. Lett. **81,** 2574 (1998).
5. Z.-Y. Li, J. Wang, and B.-Y. Gu, Phys. Rev. Lett. **81,** 2574 (1998).
6. G. Alagappan, X. W. Sun, P. Shum, and M. B. Yu, J. Opt. Soc. Am. B **23,** 1478 (2006).
7. B. Cai, T. Hattori, H. H. Deng, K. Komatsu, C. Zawadzki, N. Keil, and T. Kaino, Jpn. J. Appl. Phys. **40,** L964 (2001).
8. A. Schneider, M. Neis, M. Stillhart, B. Ruiz, R. U. A. Khan, and P. Günter, J. Opt. Soc. Am. B **23,** 1822 (2006).
9. C. Bosshard, R. Spreiter, and P. Günter, J. Opt. Soc. Am. B **18,** 1620 (2001).
10. K. Kawase, M. Mizumo, S. Sohma, H. Takahashi, T. Taniuchi, Y. Urata, S. Wada, and H. Tashiro, Opt. Lett. **24,** 1065 (1999).